Kovove Mater. 61 2023 13–21
DOI: 10.31577/km.2023.1.13

Grain refinement, texture evolutions, and strengthening of a recycled aluminium alloy subjected to tube channel pressing

Mohammad Hassan Farshidi[1]*, Muhammad Rifai[2], Hiroyuki Miyamoto[3]

[1] *Department of Materials Science and Metallurgical Engineering, Ferdowsi University of Mashhad, Azadi Square, Mashhad, Iran*
[2] *Center for Science and Technology of Advanced Materials, National Nuclear Energy Agency of Indonesia, Tangerang Selatan, Banten 15314, Indonesia*
[3] *Department of Mechanical Engineering, Doshisha University, Kyotanabe City, Kyoto, Japan*

Received 30 March 2022, received in revised form 4 November 2022, accepted 14 November 2022

Abstract

This works aims to study the grain refinement, the texture evolutions, and the strengthening of the recycled Al-1.7Fe-0.9Si-0.5Cu alloy subjected to a recently developed severe plastic deformation process called tube channel pressing. For this purpose, an electron backscattered diffraction equipped scanning electron microscope is applied to investigate the grain refinement and the texture evolutions while the tension test is applied for the measurement of strength. Results show that the imposition of the first pass of the process causes an extensive refinement of grains besides a considerable increase in strength. Despite this, the imposition of additional passes causes a little grain refinement besides a minor strength decrease. Additionally, vital texture components related to the shear deformation have risen because of the imposition of the process. Also, the mechanisms responsible for these phenomena are discussed.

K e y w o r d s: recycled aluminium, severe plastic deformation, grain refinement, strength, texture

1. Introduction

Aluminium and its alloys are widely applied because of their attractive characteristics like low density, remarkable corrosion resistance, and reasonable strength. Another attractive characteristic of these materials is their good recyclability. For instance, the energy needed for producing secondary aluminium through recycling scraps is less than 7 % of the counterpart amount needed for producing primary aluminium. Therefore, about half of aluminium products are made from secondary aluminium, and this proportion is increasing [1–3]. Despite the benefits of aluminium recycling, this process infects the composition of aluminium alloys by adding undesirable elements like Fe [1, 3–5]. For more explanations, the increased Fe-content is believed to be destructive for aluminium alloys since this element attends to the formation of different insoluble intermetallic compounds. For example, when a considerable concentration of Si besides a high Fe content is present in an aluminium alloy, different types of AlFeSi intermetallic particles form. Usually, these particles have negative effects on the mechanical properties of the alloy. For example, different alloying elements like Si, Cu, Zn, and Mg are absorbed inside these insoluble particles; therefore, the concentrations of these alloying elements inside the matrix decrease. This phenomenon causes the decrease of the strengthening effect of the alloying elements that could be attained through the formation of solid solution hardening and/or precipitation hardening [6–10]. Multiple methods proposed for eliminating recycled aluminium alloys are usually known as complicated, less effective, or expensive [4, 5–11]. Therefore, one can see the significance of applying new methods for strengthening recycled aluminium alloys bearing extraordinary Fe-contents.

During past decades, severe plastic deformation (SPD) has risen as a promising method for strengthening metallic materials. Therefore, different SPD pro-

*Corresponding author: tel.: +985138805177; e-mail address: farshidi@um.ac.ir

cesses like equal channel angular pressing (ECAP), accumulative roll bonding (ARB), and high-pressure torsion (HPT) have been established in a few past decades, different SPD processes like constraint groove pressing (CGP), tube channel pressing (TCP), and twist extrusion (TE) are still under development [12–15]. It has been well documented that applying the SPD method results in extensive grain refinement of metallic materials, usually because of continuous dynamic recrystallization (CDRX). For example, the CDRX of aluminium alloys is often explained through the following steps: initial multiplication of dislocations, migration of dislocations to form dislocation cell walls/low-angle grain boundaries, and further evolution of the low-angle grain boundaries to high-angle grain boundaries during the imposition of additional strain [16, 17]. Considering these explanations, one can see that the increase of dislocation density (ρ) and the grain refinement are two main strengthening mechanisms that arise during SPD processing of the aluminium alloys, although other strengthening mechanisms like the dynamic age-hardening and the fragmentation/redistribution of the second phase may also be occurred [18–21]. For more explanations, the strengthening effect of grain refinement can be evaluated using the Hall-Petch equation as below:

$$\Delta\sigma_{\mathrm{GB}} = K_{\mathrm{HP}} D^{-0.5}, \tag{1}$$

where D is the average grain size and K_{HP} is the Hall-Petch constant. Also, the strengthening effect of the increase of dislocation density ($\Delta\sigma_{\mathrm{dis.}}$) can be calculated as below:

$$\Delta\sigma_{\mathrm{dis.}} = \alpha M G b \rho^{0.5}, \tag{2}$$

where α is a constant of about 0.25, M is the Taylor factor of about 3.06, G is the shear modulus of the alloy, and b is its Burgers vector. The total strength of the specimens (σ_{Total}) is calculated below:

$$\sigma_{\mathrm{Total}} = \sigma_0 + \Delta\sigma_{\mathrm{dis.}} + \Delta\sigma_{\mathrm{GB}}, \tag{3}$$

where σ_0 is the frictional strength of the alloy related to other parameters like particle strengthening. For commercially pure aluminium, K_{HP}, G, and b are usually considered equal to 0.04 MPa m$^{-0.5}$, 26 GPa, and 0.286 nm, respectively [22, 23].

Besides the grain refinement, processing of the aluminium alloys by SPD causes considerable texture evolutions. This phenomenon is often interpreted considering the shear deformation texture since the SPD processes often impose the plastic strains through shear deformation. For more explanations, {1 1 1}<1 1 0> known as A, {1 1 1}<1 1 2> known as A*, {1 1 2}<1 1 0> known as B, and {0 0 1}<1 1 0> known as C are noticeable texture components risen through shear deformation of aluminium alloys. Here, the {i j k} represents the pole of the shear plane, and <h k l> represents the pole of the shear direction [24–27]. It should be considered that shear direction during an SPD process, like ECAP, depends on different parameters, such as the die design and the state of friction. For example, it is believed that two different shear vectors can occur during ECAP processing using a rounded corner die: the first shear vector (γ_β) occurs toward the channel angel bisector while the second shear vector (γ_α) occurs in the tangent direction of the die corner. The overall shear vector is calculated by adding these two shear vectors. Notably, the magnitudes of these two shear vectors depend on the state of friction. For instance, when the process is frictionless, only the γ_β occurs, and the amount of γ_α is zero. Despite this, when the frictional stress increases enough for the incidence of total sticking friction, only the γ_α occurs, and the amount γ_β is zero [27, 28].

Despite extensive studies focused on grain refinement, the strengthening, and the texture evolutions of aluminium alloys through the SPD method, the application of this method to recycled aluminium alloys bearing extraordinary Fe-content has remained less considered. This study investigates the grain refinement, texture evolution, and strengthening of a recycled Al-1.7Fe-0.9Si-0.5Cu alloy subjected to a recently developed SPD process called tube channel pressing (TCP) [23]. For this purpose, electron backscattered diffraction (EBSD) equipped scanning electron microscopy (SEM) is applied to characterize the microstructure and the texture of the alloy after the process, while the tension test is applied for the measurement of the strength.

2. Process, materials, and methods

Considering the concept of ECAP, TCP has been developed during the past decade for the SPD processing of tubes. As shown in Fig. 1a, the imposition of this process results in four steps of the shear strain besides two steps of the hoop strain. The equivalent plastic strain imposed on a tube through the applied TCP die is about 1.3, while 80 % of this amount is imposed by the shear strain steps. Each TCP shear step is similar to an ECAP process using a rounded corner die with a channel angle (Φ_{channel}) of 150°. Considering the abovementioned explanations about the shear occurrence through ECAP, possible directions of shear occurrence through the TCP process are illustrated in Fig. 1b. More details about the process and assumption of its imposed strain have been presented elsewhere [29].

A recycled aluminium alloy is received as a hot extruded tube. The inner and outer diameters of the re-

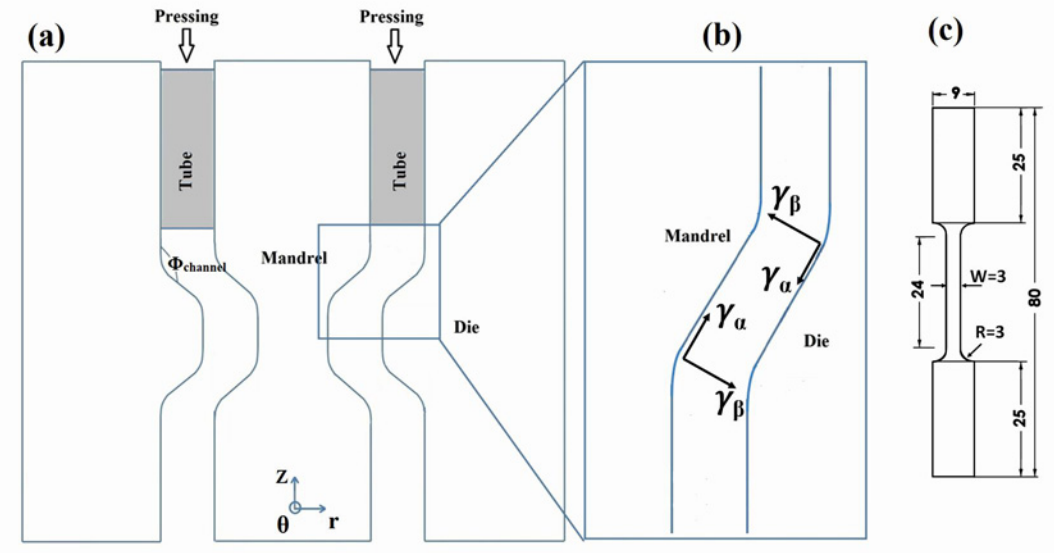

Fig. 1. Illustration of (a) schematic of the TCP process, and (b) two different possible directions of shear occurrence through this process; (c) the dimensions of the samples applied for the tension test in mm.

Table 1. Chemical composition of the received alloy (wt.%)

Al	Cr	Cu	Zr	Fe	Mg	Mn	Si	Ti	Zn
Rem.	0.01	0.49	<0.01	1.68	0.17	0.08	0.91	0.02	0.22

ceived tube are 44.4 and 50.8 mm, respectively. Table 1 illustrates the chemical composition of the received tube measured by optical emission spectrometry. As can be seen, the Fe-content of the alloy is 1.68 wt.% which is extensively greater than that of the standard aluminium alloys. Before processing by TCP, the received tube is divided into 90 mm long specimens, and these specimens are then annealed at 753 K for 45 min. Afterward, different specimens are subjected to 1 and 4 passes of TCP at room temperature. To measure the strength of the processed specimens, the tension test along the longitudinal direction of the tube is applied. The tension test is carried out at room temperature by the strain rate of $10^{-4}\,s^{-1}$ using the samples prepared according to Fig. 1c. The thickness of the tension samples is 3.2 mm, equal to the thickness of the processed tubes. Also, SEM and SEM-EBSD observations of *R-Z* planes of specimens are applied to study the evolutions of the microstructure and the texture of specimens. For this purpose, ion polishing is applied to prepare SEM-EBSD samples. The EBSD observations are accomplished by the JEOL JSM-7001F machine using the acceleration voltage of 15 kV. Different step sizes (Δx) from 0.1 to 2.5 μm are applied for EBSD mapping while grain boundaries are measured considering misorientations greater than 5° [30]. The Inca 4.09 software is applied for the interpretation of microstructure/texture evolutions of the alloy. More details about the methods of EBSD observations have been presented elsewhere [19]. The average grain misorientation (GAM) of samples obtained by EBSD is used for the estimation of the dislocation density as follows [31, 32]:

$$\rho = \frac{\mathrm{GAM}}{b\Delta x}. \tag{4}$$

3. Results and discussion

As can be seen in Fig. 2, multiple coarse intermetallic particles are present in the microstructure of the alloy. The previous work of authors on this alloy has shown that these particles are different types of AlFeSi compounds. Also, no evidence of the dissolution of these particles by TCP processing has been traced [19]. It is noteworthy that these intermetallic particles are fragmented through the TCP processing, similar to what was reported for the coarse intermetallic particles of other aluminium alloys subjected to SPD [19–21].

Figures 3–5 compare the results of SEM-EBSD observations of different specimens. As seen in Fig. 3, the grain size of the unprocessed specimen is more significant than 500 μm since the observed area ($640 \times 480\,\mu m^2$) is occupied by only one grain. This considerable coarsening of grains has probably occurred during the annealing of the alloy due to the

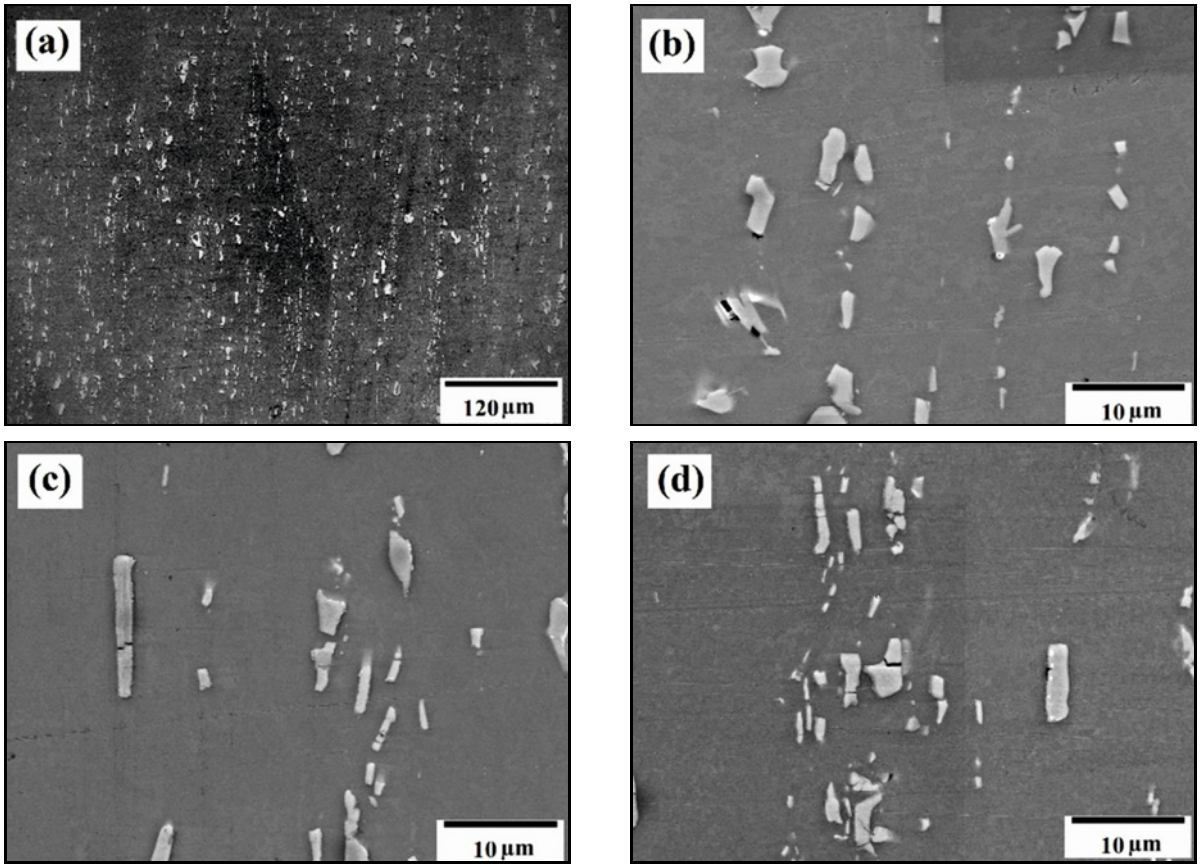

Fig. 2. Morphology of different AlFeSi intermetallic particle inside the alloy: (a) and (b) unprocessed, (c) 1 pass processed, and (d) 4 passes processed specimens.

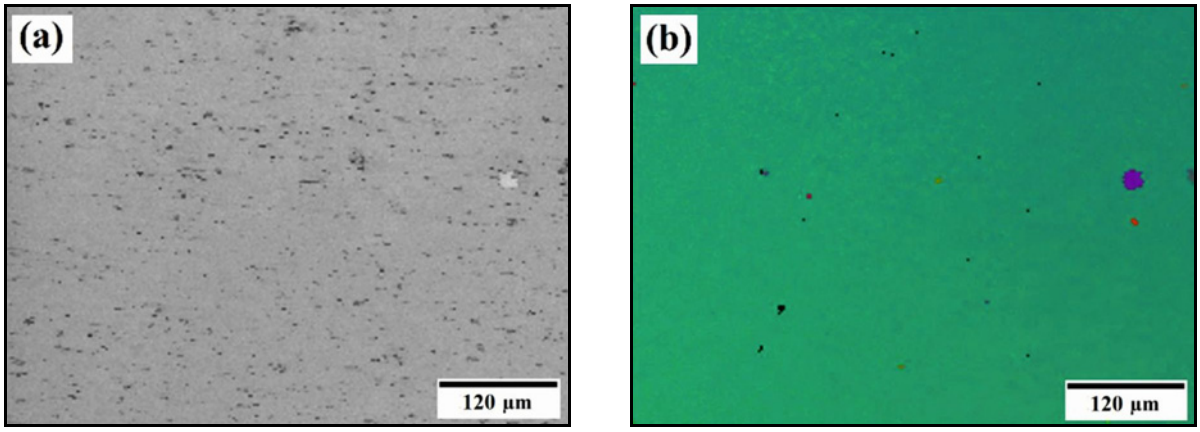

Fig. 3. EBSD results of the: (a) quality image map and (b) pole of the peripheral direction of grains of the unprocessed tube.

absence of an adequate concentration of Mn, Cr, and Zr elements in the composition of the alloy. Note that these elements are usually added to different wrought aluminium alloys to prevent their grain growth during annealing through the formation of nano-sized dispersoids [33–35]. As shown in Fig. 4, the coarse grains of the annealed alloy are broken into extensively finer grains after the 1st pass of TCP. Also, the grain sizes of the alloy after processing by 4 passes of TCP are comparable to what is seen after 1 pass of TCP. This result indicates a remarkable decrease in the rate of grain refinement through the imposition of 1 to 4 passes of TCP. It is also noteworthy that the microstructures of TCP-processed specimens are mainly occupied by very-fine grains (VFGs) characterized by diameters in the range of 1–10 µm. However,

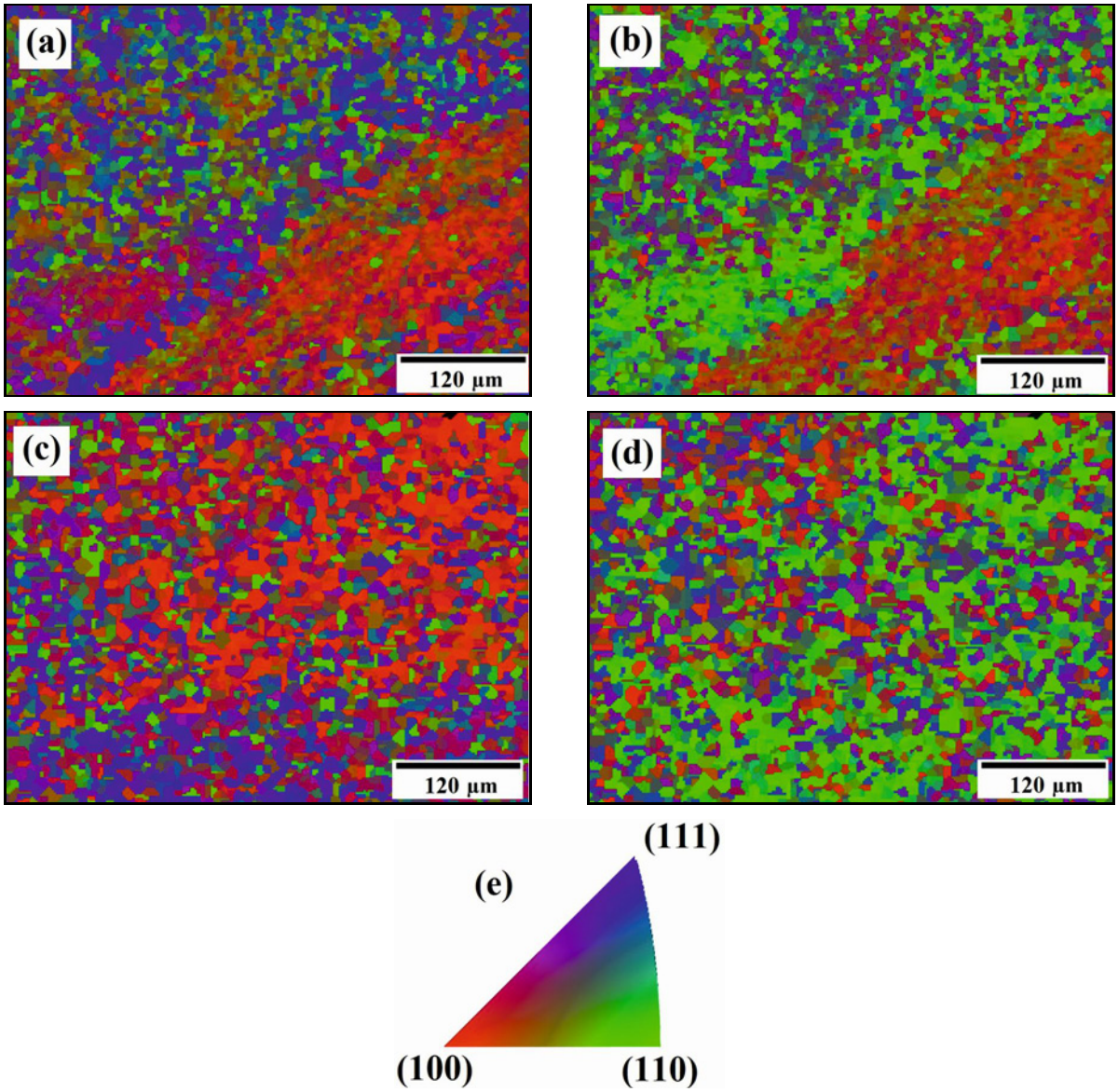

Fig. 4. Orientation image maps of grains of the alloy: (a) and (b) 1 pass processed specimen; (c) and (d) 4 passes processed specimen; (a) and (c) show poles of grains toward PD, while (b) and (d) show poles of grains toward ND; (e) legend of the orientation image maps.

when the higher magnification is applied for EBSD, a limited presence of ultrafine grains (UFG) characterized by diameters less than 1 µm is evident, as illustrated in Fig. 5. Note that these UFGs cannot be traced in Fig. 4 since the step size of EBSD mapping of Fig. 4 is greater than their diameters. As shown in Fig. 5, the UFGs induced by TCP processing often appear around intermetallic particles. This phenomenon occurs due to the greater hardness of these particles, which causes a concentration of plastic strain on the matrix around these particles [36]. Besides this, by comparing of results of this work with the results of previous studies on SPD of aluminium alloys, one can see that the grain refinement of the alloy is rapidly saturated. For more explanations, despite results of this work that shows the appearance of the VFGed microstructure inside the alloy after 4 passes of TCP processing (imposition of an equivalent plastic strain of about 5.2), previous works have reported the development of UFGed microstructures through the imposition of an equivalent plastic strain of about 4–8 on different wrought aluminium alloys [16, 17]. This phenomenon can be attributed to two different reasons. Firstly, the matrix of the recycled alloy is depleted from alloying elements because of the formation of AlFeSi intermetallic particles, and therefore, the mobility of dislocations and the occurrence of dislocations annihilation inside the matrix is extensively enhanced [6, 7, 9, 10]. This effect results in the slowing of the dislocations multiplication mechanism inside the matrix

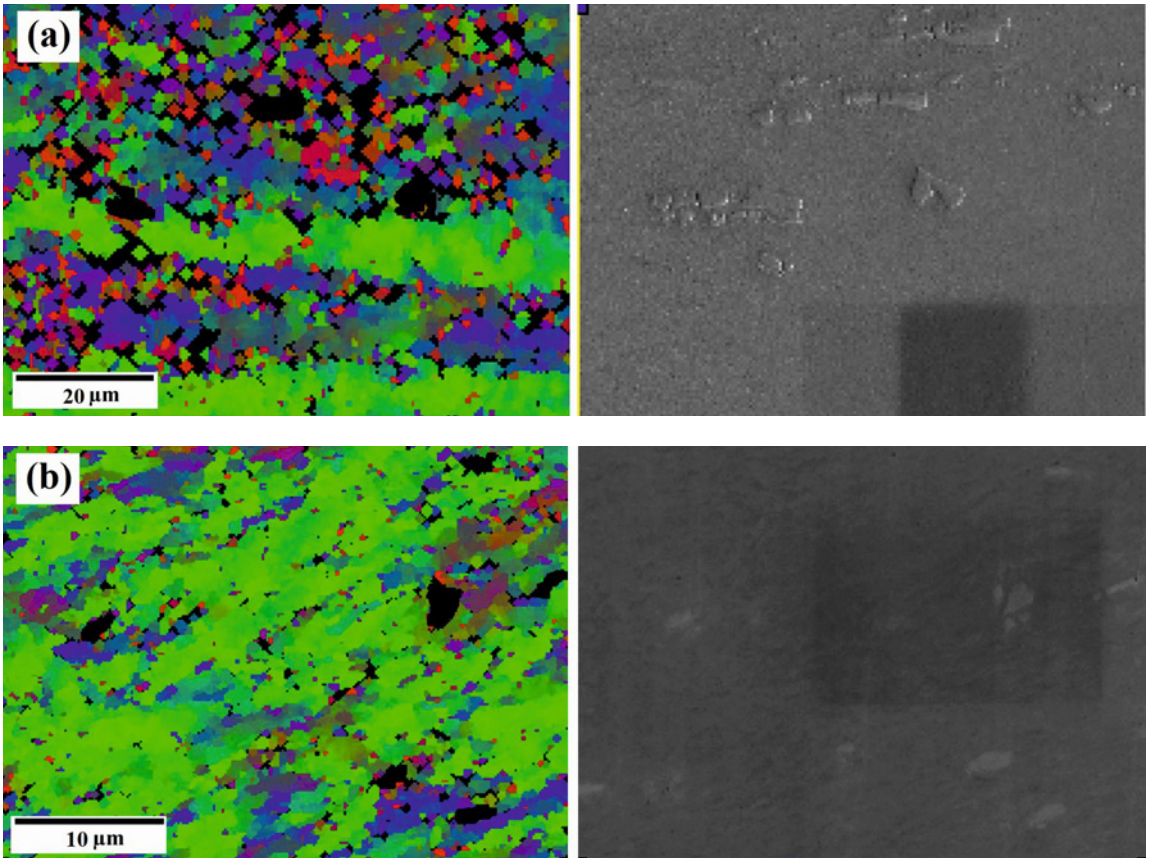

Fig. 5. Comparison of the EBSD map with the secondary electron image of the (a) 1 pass and (b) 4 passes processed specimens.

Table 2. Amount of different texture components inside the processed specimens in percentage. The figures in parentheses are the amounts of the texture components expressed as a fraction of their relative amounts in a random distribution. The data are measured using a tolerance of ± 10°

Specimen	{1 1 1} <1 1 2>	{1 1 2} <1 1 0>	{1 1 1} <1 1 0>	{0 0 1} <1 1 0>	{1 1 2} <1 1 1>	{1 1 0} <1 1 2>	{1 1 0} <1 1 1>	{1 1 0} <0 0 1>
1 Pass	<1 (<1)	5.7 (4.2)	3.9 (2.9)	<1 (<1)	<1 (<1)	1.2 (<1)	<1 (<1)	<1 (<1)
4 Passes	<1 (<1)	5.2 (3.9)	3.4 (2.6)	7.3 (10.4)	<1 (<1)	<1 (<1)	<1 (<1)	<1 (<1)

that is essential for the occurrence of CDRX of aluminium [16, 17]. Secondly, the absence of nano-sized dispersoids – usually composed of Mn, Cr, and Zr – inside the alloy causes enhancement of the mobility of its grain boundaries, and therefore, the coalescence of grains by the migration of their boundaries during SPD is accelerated [37].

As seen in Fig. 4, the pole of pressing direction (PD) of multiple grains of processed specimens is near <1 1 0>. Additionally, the pole of average direction (ND) of multiple grains of processed specimens is near to <1 1 1> or <1 0 0>. These results imply the appearance of relatively vital texture components through TCP processing of the alloy. Note that the PD and the ND are identical to the longitudinal and radial directions of the tube, respectively. Table 2 illustrates the fraction of risen texture components inside the processed specimens. Here, the {i j k} represents the pole of ND, and <h k l> represents the pole of PD. As can be traced in Table 2, supposing the pole of the shear plane and pole of the shear direction identical to ND and PD, the texture components risen through TCP processing are equal to A, B, and C components of the shear texture mentioned above. Notably, the intensities of other texture components inside the processed specimens are less than their intensities in a random texture. These results indicate the appearance of the shear texture through processing by TCP. Furthermore, considering these explanations, one can infer that the shear deformation dur-

Table 3. Comparison of the microstructural characteristics and different strengthening parameters of specimens

Pass number	D (μm)	ρ (1 m^{-2})	$\Delta\sigma_{GB}$	$\Delta\sigma_{dis.}$	σ_{Total}	$\sigma_{ex.}$
0	~500	~3.3 × 10^{13}	2	32	49	45
1	2.3	9.1 × 10^{14}	28	169	212	231
4	1.4	7 × 10^{14}	36	147	208	199

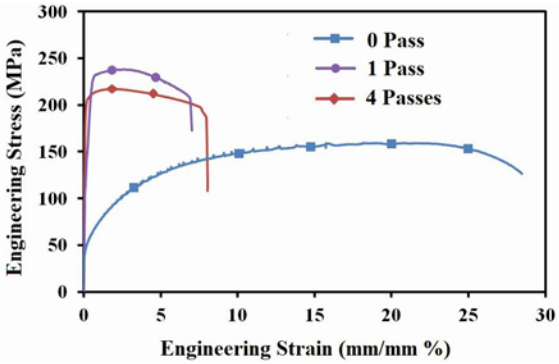

Fig. 6. Results of the tension tests of different specimens.

ing the applied TCP process mainly occurs toward PD while the pole of the shear plane is ND. Comparing this result with the possible directions of shear through TCP processing illustrated in Fig. 1b, it can be inferred that the primary shear vector of TCP is aligned to γ_α, and therefore, one can infer that the γ_β is negligible. This phenomenon can be interpreted as full sticking friction between the specimen and the die [28]. Note that the proportion of length to thickness of the applied tube is 28 and the tube surface is in complete contact with die/mandrel surfaces throughout the process, as shown in the authors' previous work [29]. These phenomena result in the imposition of significant backpressure on the tube during TCP processing, even using perfect lubrication. Therefore, the hydrostatic pressure and the friction stress between the surfaces of the die/mandrel versus the surface of the tube increases extensively. As a result, full sticking friction occurs, similar to what was reported in previous studies [38, 39].

Figure 6 illustrates the results of the tension tests of different specimens. As can be seen, the imposition of TCP causes a considerable increase in the yield strength of the alloy. This strength increase is mainly attributed to the increase in the dislocation density and the grain refinement, as discussed above. As shown in Fig. 6, the yield strength of 4 passes processed specimen is lower than the strength of 1 pass processed specimen. To understand this effect, one can compare the strength of the specimens evaluated considering Eqs. (1)–(4) and the experimentally obtained strength ($\sigma_{ex.}$) of the specimens. Table 3 compares the average grain size and the dislocation density evaluated by EBSD versus the related strengthening effect of these characteristics for different specimens. Note that the σ_0 is considered equal to 15 MPa. As can be seen in Table 3, while the $\sigma_{ex.}$ of the 1 pass processed specimen is a bit higher than its σ_{Total}, the $\sigma_{yl.}$ of 4 passes processed specimen is lower than its σ_{Total}. Considering the abovementioned results about the texture evolutions of the alloy through TCP, one may associate this difference of the specimens to the texture risen through the process. For more explanations, the imposition of 4 passes of TCP causes an extensive increase in fraction of C texture component, as shown in Table 2. On the other hand, the Schmidt factor of the C texture component through the applied tension test is 0.408. This number is considerably more significant than the average amount of Schmidt factor in a random texture of about 0.33 [40, 41]. Therefore, the C texture component is weaker during the applied tension test, and increased fraction of this texture component after the imposition of 4 passes of TCP causes the decrease of strength of the alloy.

4. Conclusions

Considering the results of this study on SPD of a recycled aluminium alloy bearing an extraordinary Fe-content, the following conclusions are summarized:

1. The grain refinement of the alloy through the SPD is rapidly saturated compared to what is seen for the conventional wrought aluminium alloys.

2. A relatively firm shear texture appears through the imposition of the applied TCP process due to the occurrence of shear in the tangent direction of the die corner.

3. The imposition of 1 pass of TCP causes a considerable increase in the strength of the alloy. However, the imposition of other additional TCP passes causes a minor decrease in the strength of the alloy related to the texture component persuaded by the process.

Acknowledgements

The corresponding author wishes to thank the Ferdowsi University of Mashhad (FUM) research board for the financial support and the provision of research facilities

used in this work through grant No. 2/53696. The authors also wish to thank the research board of Doshisha University for providing research facilities used in this work.

References

[1] S. Capuzzi, G. Timelli, Preparation and melting of scrap in aluminum recycling: A review, Metals 8 (2018) 249. https://doi.org/10.3390/met8040249

[2] J. Blomberg, P. Soderholm, The economics of secondary aluminium supply: An econometric analysis based on European data, Resources, Conservation and Recycling 53 (2009) 455–463. https://doi.org/10.1016/j.resconrec.2009.03.001

[3] H. Lu, Z. Hou, M. Ma, G. Lu, Effect of Fe-content on the mechanical properties of recycled Al alloys during hot compression, Metals 7 (2017) 262. https://doi.org/10.3390/met7070262

[4] C. Chen, J. Wang, D. Shu, P. Li, J. Xue, B. Sun, A novel method to remove iron impurity from aluminum, Materials Transactions 52 (2011) 1629–633 https://doi.org/10.2320/matertrans.M2011108

[5] G. Gaustada, E. Olivetti, R. Kirchain, Improving aluminum recycling: A survey of sorting and impurity removal technologies, Resources, Conservation and Recycling 58 (2012) 79–87. https://doi.org/10.1016/j.resconrec.2011.10.010

[6] L. Sweet, S. M. Zhu, S. X. Gao, J. A. Taylor, M. A. Easton, The effect of iron content on the iron-containing intermetallic phases in a cast 6060 aluminum alloy, Metallurgical and Materials Transaction A 42 (2011) 1737–1749. https://doi.org/10.1007/s11661-010-0595-6

[7] H. W. Kim, S. B. Kang, N. Tsuji, Y. Minamino, Elongation increase in ultra-fine grained Al-Fe-Si alloy sheets, Acta Materialia 53 (2005) 1737–1749. https://doi.org/10.1016/j.actamat.2004.12.022

[8] S. R. Wagstaff, The impact of recycling on the mechanical properties of 6xxx series aluminum alloys, Journal of Siberian Federal University: Engineering & Technologies 11 (2018) 409–418. http://dx.doi.org/10.17516/1999-494X-0063

[9] H. Yang, S. Ji, Z. Fan, Effect of heat treatment and Fe content on the microstructure and mechanical properties of die-cast Al-Si-Cu alloys, Materials and Design 85 (2015) 823–832. http://dx.doi.org/10.1016/j.matdes.2015.07.074

[10] M. F. Ibrahim, A. M. Samuel, F. H. Samuel, A preliminary study on optimizing the heat treatment of high strength Al-Cu-Mg-Zn alloys, Materials and Design 57 (2014) 342–350. https://doi.org/10.1016/j.matdes.2013.11.078

[11] L. Zhang, J. Gao, L. Nana, W. Damoah, D. G. Robertson, Removal of iron from aluminum: A review, Mineral Processing and Extractive Metallurgy Review 33 (2012) 99–157. https://doi.org/10.1080/08827508.2010.542211

[12] Y. Estrin, A. Vinogradov, Extreme grain refinement by severe plastic deformation: A wealth of challenging science, Acta Materialia 61 (2013) 782–817. https://doi.org/10.1016/j.actamat.2012.10.038

[13] M. H. Farshidi, M. Kazeminezhad, The effects of die geometry in tube channel pressing: Severe plastic deformation, Proc IMechE Part L: J. Materials: Design and Applications 230 (2016) 263–272. https://doi.org/10.1177/1464420715569289

[14] E. N. Moskvichev, V. A. Skripnyak, V. V. Skripnyak, A. A. Kozulin, D. V. Lychagin, Structure and mechanical properties of aluminum 1560 alloy after severe plastic deformation by groove pressing, Physical Mesomechanics 21 (2018) 515–522. https://doi.org/10.1134/S1029959918060061

[15] J. Joudaki, M. Safari, S. M. Alhossein, Hollow twist extrusion: introduction, strain distribution, and process parameters investigation, Metal and Materials International 25 (2019) 1593–1602. https://doi.org/10.1007/s12540-019-00301-7

[16] I. Sabirov, M. Y. Murashkin, R. Z. Valiev, Nanostructured aluminium alloys produced by severe plastic deformation: New horizons in development, Materials Science and Engineering A 560 (2013) 1–24. https://doi.org/10.1016/j.msea.2012.09.020

[17] T. Sakai, A. Belyakov, R. Kaibyshev, H. Miura, J. J. Jonas, Dynamic and post-dynamic recrystallization under hot, cold and severe plastic deformation conditions, Progress in Materials Science 60 (2014) 130–207. https://doi.org/10.1016/j.pmatsci.2013.09.002

[18] R. Bakhshi, M. H. Farshidi, S. A. Sajjadi, Strengthening of aluminium alloy 7005 through imposition of severe plastic deformation supplemented by different ageing treatments, Transactions of Nonferrous Metals Society of China 31 (2021) 2909–2921. https://doi.org/10.1016/S1003-6326(21)65702-3

[19] M. H. Farshidi, M. Rifai, H. Miyamoto, Microstructure evolution of a recycled Al-Fe-Si-Cu alloy processed by tube channel pressing, International Journal of Minerals, Metallurgy and Materials 25 (2018) 1166–1172. https://doi.org/10.1007/s12613-018-1668-6

[20] I. Gutierrez-Urrutia, M. A. Muños-Morris, D. G. Morris, Contribution of microstructural parameters to strengthening in an ultrafine-grained Al-7%Si alloy processed by severe deformation, Acta Materialia 55 (2007) 1319–1330. https://doi.org/10.1016/j.actamat.2006.09.037

[21] C. Xu, M. Furukawa, Z. Horita, T. G. Langdon, Influence of ECAP on precipitate distributions in a spray-cast aluminum alloy, Acta Materialia 53 (2005) 749–758. https://doi.org/10.1016/j.actamat.2004.10.026

[22] T. Koizumi, M. Kuroda, Grain size effects in aluminum processed by severe plastic deformation, Materials Science and Engineering A 710 (2018) 300–308. https://doi.org/10.1016/j.msea.2017.10.077

[23] N. Hansen, Hall-Petch relation and boundary strengthening, Scripta Materialia 51 (2004) 801–806. https://doi.org/10.1016/j.scriptamat.2004.06.002

[24] S. Li, I. J. Beyerlein, M. A. M. Bourke, Texture formation during equal channel angular extrusion of fcc and bcc materials: Comparison with simple shear, Materials Science and Engineering A 394 (2005) 66–77. https://doi.org/10.1016/j.msea.2004.11.032

[25] D. Orlov, P. P. Bhattacharjee, Y. Todaka, M. Umemoto, N. Tsuji, Texture evolution in pure aluminum subjected to monotonous and reversal straining in high-pressure torsion, Scripta Materialia 60 (2009) 893–896. https://doi.org/10.1016/j.scriptamat.2009.02.004

[26] X. H. Fan, D. Tang, W. L. Fang, D. Y. Li, Y. H. Peng, Microstructure development and texture evolution of aluminum multi-port extrusion tube during the porthole die extrusion, Materials Characterization 118 (2016) 468–480. https://doi.org/10.1016/j.matchar.2016.06.025

[27] I. J. Beyerlein, L. S. Toth, Texture evolution in equal--channel angular extrusion, Progress in Materials Science 54 (2009) 427–510. https://doi.org/10.1016/j.pmatsci.2009.01.001

[28] A. P. Zhilyaev, K. Oh-Ishi, G. I. Raab, T. R. McNelley, Influence of ECAP processing parameters on texture and microstructure of commercially pure aluminum, Materials Science and Engineering A 441 (2006) 245–252. https://doi.org/10.1016/j.msea.2006.08.029

[29] M. H. Farshidi, Optimization of die geometry for tube channel pressing, Iranian Journal of Materials Forming 5 (2018) 26–35. https://dx.doi.org/10.22099/ijmf.2018.26954.1093

[30] N. Kamikawa, X. Huang, N. Tsuji, N. Hansen, Strengthening mechanisms in nanostructured high--purity aluminium deformed to high strain and annealed, Acta Materialia 57 (2009) 4198–4208. https://doi.org/10.1016/j.actamat.2009.05.017

[31] M. Calcagnotto, D. Ponge, E. Demir, D. Raabe, Orientation gradients and geometrically necessary dislocations in ultrafine grained dual-phase steels studied by 2D and 3D EBSD, Materials Science and Engineering A 527 (2010) 2738–2746. https://doi.org/10.1016/j.msea.2010.01.004

[32] P. J. Konijnenberg, S. Zaefferer, D. Raabe, Assessment of geometrically necessary dislocation levels derived by 3D EBSD, Acta Materialia 99 (2015) 402–414. https://doi.org/10.1016/j.actamat.2015.06.051

[33] M. Kenyon, J. Robson, J. Fellowes, Z. Liang, Effect of dispersoids on the microstructure evolution in Al-Mg--Si alloys, Advanced Engineering Materials 21 (2018) 1800494. http://dx.doi.org/10.1002/adem.201800494

[34] P. Z. Zhao, T. Tsuchida, Effect of fabrication conditions and Cr, Zr contents on the grain structure of 7075 and 6061 aluminum alloys, Materials Science and Engineering A 499 (2009) 78–82. http://dx.doi.org/10.1016/j.msea.2007.09.094

[35] D. Tsivoulas, P. B. Prangnell, The effect of Mn and Zr dispersoid-forming additions on recrystallization resistance in Al-Cu-Li AA2198 sheet, Acta Materialia 77 (2014) 1–16. https://doi.org/10.1016/j.actamat.2014.05.028

[36] P. J. Apps, J. R. Bowen, P. B. Prangnell, The effect of coarse second-phase particles on the rate of grain refinement during severe deformation processing, Acta Materialia 51 (2003) 2811–2822. https://doi.org/10.1016/S1359-6454(03)00086-7

[37] R. Pippan, S. Scheriau, A. Taylor, M. Hafok, A. Hohenwarter, A. Bachmaier, Saturation of fragmentation during severe plastic deformation, Annual Review of Materials Research, 40 (2010) 319–343. https://doi.org/10.1146/annurev-matsci-070909-104445

[38] F. Widerøe, T. Welo, Conditions for sticking friction between aluminium alloy AA6060 and tool steel in hot forming, Key Engineering Materials 491(2012) 121–128. https://doi.org/10.4028/www.scientific.net/KEM.491.121

[39] I. Flitta, T. Sheppard, Nature of friction in extrusion process and its effect on material flow, Materials Science and Technology 19 (2003) 837–846. https://doi.org/10.1179/026708303225004422

[40] J. Hirsch, T. Al-Samman, Superior light metals by texture engineering: Optimized aluminum and magnesium alloys for automotive applications, Acta Materialia 61 (2013) 818–843. https://doi.org/10.1016/j.actamat.2012.10.044

[41] M. Moghaddam, A. Zarei-Hanzaki, M. H. Pishbin, A. H. Shafieizad, V. B Oliveira, Characterization of the microstructure, texture and mechanical properties of 7075 aluminum alloy in early stage of severe plastic deformation, Materials Characterization 119 (2016) 137–147. https://doi.org/10.1016/j.matchar.2016.07.026